AGU PUBLICATIONS

Geophysical Research Letters

RESEARCH LETTER
10.1002/2016GL068282

Key Points:
- Multipolarization SAR image processing for oil slick discrimination
- Internal calibration of the image processing with respect to incidence angle
- Oil slicks and oil spills in the marine environment

Correspondence to:
D. V. Ivonin,
ivonin@ocean.ru;
ivanoff@ocean.ru

Citation:
Ivonin, D. V., S. Skrunes, C. Brekke, and A. Yu. Ivanov (2016), Interpreting sea surface slicks on the basis of the normalized radar cross-section model using RADARSAT-2 copolarization dual-channel SAR images, *Geophys. Res. Lett., 43*, 2748–2757, doi:10.1002/2016GL068282.

Received 15 FEB 2016
Accepted 1 MAR 2016
Accepted article online 6 MAR 2016
Published online 24 MAR 2016

Interpreting sea surface slicks on the basis of the normalized radar cross-section model using RADARSAT-2 copolarization dual-channel SAR images

D. V. Ivonin[1,2], S. Skrunes[3], C. Brekke[3], and A. Yu. Ivanov[1]

[1]P.P. Shirshov Institute of Oceanology, Russian Academy of Sciences, Moscow, Russia, [2]Russian State Hydrometeorological University, Satellite Oceanography Laboratory, Saint-Petersburg, Russia, [3]Department of Physics and Technology, University of Tromsø-The Arctic University of Norway, Tromsø, Norway

Abstract A simple automatic multipolarization technique for discrimination of main types of thin oil films (of thickness less than the radio wave skin depth) from natural ones is proposed. It is based on a new multipolarization parameter related to the ratio between the damping in the slick of specially normalized resonant and nonresonant signals calculated using the normalized radar cross-section model proposed by Kudryavtsev et al. (2003a). The technique is tested on RADARSAT-2 copolarization (VV/HH) synthetic aperture radar images of slicks of a priori known provenance (mineral oils, e.g., emulsion and crude oil, and plant oil served to model a natural slick) released during annual oil-on-water exercises in the North Sea in 2011 and 2012. It has been shown that the suggested multipolarization parameter gives new capabilities in interpreting slicks visible on synthetic aperture radar images while allowing discrimination between mineral oil and plant oil slicks.

1. Introduction

Oil spill identification and characterization remains a challenge for the modern remote sensing. The satellite synthetic aperture radars (SAR) seem to be the most efficient instruments for providing weather and daylight-independent information about the sea surface conditions including oil pollution. Films of mineral oils, i.e., crude oil, its emulsions, and different oil products, are visible on SAR images as dark spots surrounded by the brighter sea surface. However, natural phenomena, such as biogenic films, thin ice, and low wind, form a variety of so-called look-alikes frequently resulting in false detections. Distinguishing oil spills from look-alikes on SAR images remains a significant unsolved problem of modern ocean remote sensing.

Accordingly, many researchers are searching for a way to develop a method that could deal with SAR data automatically in a routine manner. Processing of multipolarization radar data is considered to be very promising in this context. Among recent prominent examples we note, e.g., (i) the copolarized phase difference method proposed by *Migliaccio et al*. [2009] and *Velotto et al*. [2011], (ii) the conformity coefficient μ proposed by *Zhang et al*. [2011], and (iii) decomposition parameters, such as the entropy, H, and the mean scattering angle, α. However, it was shown that these parameters could vary strongly within the same slick depending on the incidence angle [see *Minchew et al*., 2012, Figures 14–16; *Skrunes et al*., 2014, Figure 9, hereinafter *S*2014].

In this paper we demonstrate how the model of the normalized radar cross section (NRCS) proposed in *Kudryavtsev et al*. [2003a, hereinafter *K*2003a] could help to advance toward a slick discrimination method suitable for operational purposes, which could treat slicks visible on SAR images independently of incidence angles, the sensor frequency band, etc. The model takes into account both the resonant part of the backscattered signal, provided by the Bragg mechanism and caused by the short gravity-capillary wind waves, and a nonresonant part, provided by reflections from sharp patches on the sea surface caused by wave breaking. These theoretical findings strongly extended our understanding of multipolarization features of various oceanic slicks prompted by the seminal works by *Gade et al*. [1998a, 1998b] based on consideration of the resonant part of the signal.

Here we propose a simple copolarization dual-channel technique following an idea of *Kudryavtsev et al*. [2013, hereinafter *K*2013], which uses the ratio between the normalized resonant and nonresonant signals within the slick to classify its nature. The main and key difference of the technique described in this paper from the previous ones [*Migliaccio et al*., 2009; *Velotto et al*., 2011; *Zhang et al*., 2011; *Skrunes et al*., 2015b,

hereinafter *S2015*b; *K*2013] is that we try to propose a single *quantity*, which would not depend on the incidence angle and would have theoretically predictable behavior with respect to other parameters such as weather conditions and frequency band. As a first step, it has been shown that independence of the incidence angle can be achieved, although with some limitations, which will confine possible applications of the technique to a range of medium incidence angles.

The method was tested on RADARSAT-2 (R-2) copolarization (VV and HH) images acquired in quad-polarimetric mode (HH/HV/VH/VV) in conjunction with annual oil-on-water exercises at the abandoned "Frigg field" in the North Sea in 2011 and 2012, containing controlled releases of crude oil, emulsion, and plant oil where the plant oil was used to model a biogenic slick.

2. Model Approach

The normalized radar cross-section model of the copolarized (VV and HH) scattering from the sea surface developed in *K*2003a is the starting point for the development of the methodology proposed here. The model takes into account three polarization terms: (1) σ_B is the conventional two-scale resonant Bragg scattering from the short gravity-capillary wind waves, (2) σ_{sp} is the nonpolarized specular Kirchhoff reflection from slopes of long waves, and (3) σ_n is the nonpolarized scattering, according to *K*2003a, due to a nonresonant scattering from the rough surface patches caused by wave breaking. The NRCS for copolarization channels, vertical, σ^V, or horizontal, σ^H, is thus defined as

$$\begin{aligned} \sigma^V &= \sigma_B + \sigma_{sp} + \sigma_n \\ \sigma^H &= P_B\sigma_B + \sigma_{sp} + \sigma_n. \end{aligned} \tag{1}$$

Here

$$\sigma_B = 16\pi k_r^4 |G_V(\theta,\varepsilon)|^2 F(k_b)\left(1 + g_V\zeta_i^2\right) \tag{2}$$

is the two-scale Bragg scattering term for the vertical polarization, and $|G_V(\theta,\varepsilon)|^2$ is the scattering coefficient depending on the incidence angle, θ, and the water dielectric constant, ε; $F(k_b)$ is the spectrum of short gravity-capillary waves, $k_b = 2k_r \sin\theta$ is the Bragg wave number, k_r is the SAR wave number, and ζ_i^2 is the mean square slopes of long tilting waves. The polarization coefficient P_B reflects the fact that the Bragg scattering part depends on the polarization. $P_B \approx P_{0B}\left[1 + (g_H - g_V)\zeta_i^2\right]$, where $P_{0B} = |G_H|^2/|G_V|^2$ and $g_{V,H} = 1/2 \cdot \partial^2|G_{V,H}|/\partial\theta^2$ (*K*2003a).

NRCS of the specular reflections from slopes of long waves, σ_{sp}, is [*Valenzuela*, 1978]

$$\sigma_{sp}(\theta) = |R|^2 \frac{\sec^4\theta}{\zeta_\perp\zeta_i} \exp\left(-\frac{\tan^2\theta}{\zeta_i^2}\right), \tag{3}$$

where R is the Frenel reflection coefficient at normal incidence, ζ_i^2 is the mean square slope of waves supporting specular reflection in the direction of incidence plane, ζ_i is the corresponding standard deviation, and $\zeta_\perp$ is the standard deviation of slope of these waves in the direction perpendicular to the incidence plane.

The last term, σ_n, initially, was introduced in relation to wave breakings [*Kwoh and Lake*, 1984; *Banner and Fooks*, 1985; *Ericson et al*., 1999; *K*2003a] and the length of the wave breaking fronts [*Phillips*, 1988]. This point drew a great portion of criticism from the scientific community, especially for winds as low as 2–4 m/s. Nevertheless, it was experimentally shown that at even such low winds there are always breakings, although without white caps, so-called *microbreakings* [*Caulliez and Guérin*, 2012; *Caulliez*, 2013], which could cause sufficiently high nonresonant backscattering [*Ericson et al*., 1999; *Churyumov et al*., 2002]. The role of the nonpolarized scattering due to the wave breakings varies depending on the frequency band. For example, it contributes about 40% to the total NRCS at HH polarization for C band and wind speed 5 m/s [*Kudryavtsev et al*., 2003b] but becomes negligible for L band where the Bragg mechanism dominates [*Kudryavtsev et al*., 2003b; *Minchew et al*., 2012]. It will be shown below that σ_n contributes to the total NRCS about 40–70% in our data. Hereinafter, we will refer to this nonpolarized term σ_n as a nonresonant scattering from *short-scale* (in comparison to the long surface gravity waves) *rough surface patches* (RSPs) caused by wave breakings and microbreakings, independently on whether they are accompanied by the whitecapping or not. The nonresonant term, σ_n, is described as follows (see details in *K*2003a):

$$\sigma_n = q\cdot|R|^2\sigma_{0n}(\theta)\,,$$
$$\sigma_{0n}(\theta) = \left(\sec^4\theta/s_n^2\right)\exp\left(-\tan^2\theta/s_n^2\right) + \varepsilon_n/s_n^2. \tag{4}$$

Here q is the fraction of the sea surface covered by RSP; it is described as an integral of lengths of wave breaking fronts per unit surface expressed through the short wind wave spectrum $F(k_b)$. $\sigma_{0n}(\theta)$ describes the mechanism of specular reflections from RSP. It has a form similar to (3) and depends on the incidence angle. $s_n^2 = 0.19, \varepsilon_n = 0.005$ are the empirical coefficients used to fit experimental data. We added here the Fresnel reflection coefficient, R, at normal incidence that has to account for the dielectric properties of oil and water in the general case of thick films.

For simplicity of our analysis we considered the SAR images only where the specular reflections, σ_{sp}, from slopes of long waves are negligible in comparison with the other terms. The works [*Valenzuela*, 1978; *K*2003a] say that for clean water the specular reflections, σ_{sp}, are often negligible in comparison to other terms if an incidence angle is greater than 20°. It will be shown in section 5 that for slicks in C band at wind speeds less than 6 m/s and incidence angle greater than 27° the specular reflections, σ_{sp}, can be neglected with respect to the nonresonant part of the signal, σ_n. Consequently, in such approximation one gets the following expressions for the resonant and nonresonant parts:

$$\sigma_B = \frac{\sigma^V - \sigma^H}{1 - P_{0B}}, \sigma_n \approx \frac{\sigma^H - P_{0B}\sigma^V}{1 - P_{0B}}. \tag{5}$$

(For the resonant, Bragg, part it is exact and there is no need to neglect tilting [*Guérin et al*., 2010]; for the nonresonant part it is approximate due to neglecting the effect of tilting waves on the polarization coefficient.) Here the principal point is that with the help of the known polarization coefficient, $P_{0B}(\theta)$, we eliminate the dependency of σ_B and σ_n on the incidence angle. This operation can be considered as a first step of the internal calibration of the signals with respect to incidence angle. To complete the calibration, we introduce the damping factors $\widetilde{\sigma}_B$ and $\widetilde{\sigma}_n$ for resonant and nonresonant signals relative to their values at clean water

$$\widetilde{\sigma}_B = \frac{\sigma_{B,\text{slick}}}{\sigma_{B,\text{water}}}, \widetilde{\sigma}^n = \frac{\sigma_{n,\text{slick}}}{\sigma_{n,\text{water}}}. \tag{6}$$

Here $\sigma_{B,\text{slick}}$ and $\sigma_{n,\text{slick}}$ are "slick" intensities within the dark patch. $\sigma_{B,\text{water}}$ and $\sigma_{n,\text{water}}$ are "clean water" normalization parameters, which are mean intensities for the part of SAR image not containing the dark patch (for details see section 4).

It was shown in *Franceschetti et al*. [2002, hereinafter *F*2002] for C band (5.6 GHz) that the dielectric constant of oil (which is an order of magnitude smaller than that for water) had a negligible effect on the reflection coefficients R, G_V, and G_H for oil surface layers with thicknesses smaller than 2 mm (if the incidence angle is less than 70°). The reflection coefficients become sensitive to the dielectric constant of oil only in the case of very thick films, as it was, for example, for the "Deepwater Horizon" when the oil raised from depth 1.7 km to reach the surface [*North et al*., 2011], and "the upper layer of the ocean surface was likely a mixture of water and oil" [*Minchew et al*., 2012]. Therefore, it was a case of *thick* slick where the thickness of oil-water mixture was estimated to be greater than the skin depth of the radio wave (i.e., greater than 7–9 mm in the case of L band) [*Minchew et al*., 2012]. We concentrate our study on *thin* slicks with thicknesses less than the skin depth (which is 2–4 mm for sea water at C band) [*Ulaby et al*., 1986; *F*2002; *S2015b*].

In accordance with *F*2002, for the case when the film thicknesses are less than the skin depth and the incidence angle is less than 70° we can neglect the dependence on dielectric constant and ignore the variations of the coefficients R, G_V, G_H, and P_{0B} over the slick. Therefore, in this approximation, the damping factors $\widetilde{\sigma}_B$ and $\widetilde{\sigma}_n$ should be proportional to a suppression of short gravity-capillary waves in the slick and to a suppression of the fraction of sea surface area covered by RSP in the slick, correspondingly, i.e.,

$$\widetilde{\sigma}_B = \frac{F(k_b)_{\text{slick}}}{F(k_b)_{\text{water}}}, \widetilde{\sigma}_n = \frac{q_{\text{slick}}}{q_{\text{water}}}. \tag{7}$$

Here the only, relatively weak, dependence on the incidence angle remains in the Bragg wave number $k_b = 2k_r \sin\theta$. While the incidence angle is changing from 30° to 40°, there is a 30% change in the Bragg wave number, and the corresponding value $F(k_b)$ changes less than 10% for C band in wind speeds of 3–10 m/s [see

Elfouhaily et al., 1997; *Yurovskaya et al*., 2013; *K*2003a]. According to the integral form of determination of the fraction, q, of sea surface area covered by RSP [*K*2003a] its dependence on k_b and the incidence angle may be considered to be negligible in our approach. Equation (7) stresses the role of the simple normalizations (5) and (6), which allow us to get rid of most of the dependence on the incidence angle and emphasize the dependence of parameters $\widetilde{\sigma}_B$ and $\widetilde{\sigma}_n$ on the slick properties and weather conditions only.

As a result of performing the normalizations using equations (5) and (6), we assume that the calculated damping factors $\widetilde{\sigma}_B$ and $\widetilde{\sigma}_n$ should depend only slightly on the incidence angle, as opposed to the initial images σ^V and σ^H, the entropy, H, mean scattering angle, α, and other polarimetric decomposition parameters that are sensitive to the incidence angle. We use these calibrated polarimetric parameters $\widetilde{\sigma}_B$ and $\widetilde{\sigma}_n$ to create a two-dimensional scattering plot. Such diagrams are widely accepted when dealing with other polarimetric parameters (see, e.g., *S*2014). The main advantage of dealing with $\widetilde{\sigma}_B$ and $\widetilde{\sigma}_n$ is that for a given type of slick and thickness, the location in the scatter plot should be the same for images obtained over a range of incident angles (in the same frequency band).

After a calibration with respect to the incidence angle, a robust parameter depending only on the slick type but not the slick thickness can be introduced using $\widetilde{\sigma}_B$ and $\widetilde{\sigma}_n$. The absolute values of the damping factors $\widetilde{\sigma}_B$ and $\widetilde{\sigma}_n$ depend on the slick thickness. Therefore, to get rid of the absolute values of $\widetilde{\sigma}_B$ and $\widetilde{\sigma}_n$, we propose to use the ratio of the resonant and nonresonant components relative damping (*RND)*

$$\mathrm{RND} = \Delta\widetilde{\sigma}_n / \Delta\widetilde{\sigma}_B, \tag{8}$$

where $\Delta\widetilde{\sigma}_n = 1 - \widetilde{\sigma}_n$ and $\Delta\widetilde{\sigma}_B = 1 - \widetilde{\sigma}_B$ are the relative damping of resonant and nonresonant components, respectively. Here we assumed that the slick suppresses short waves and short-scale rough surface patches in the same proportion for some range of slick thicknesses. Accordingly, the parameter RND is assumed not to vary much in the range of typical thicknesses for one slick type. Thus, it should contain mainly the information about the slick type and can generally be used within the range of incidence angles and oil spill thicknesses here under consideration, respectively.

3. Field Data

The proposed technique was applied to two R-2 images acquired during oil-on-water exercises in the North Sea in 2011 and 2012 with controlled crude oil, emulsion, and plant oil spills (see Figure 1). All the processed images were collected in the quad-polarization mode: they were R-2 Fine Quad-pol SLC (single look complex) product [*MDA*, *Geospatial Service*, 2014]. For slick classification we used the copolarization images only (VV and HH) because we had no need in cross-polarization terms (VH and HV) for the copolarization technique described in (5), (6), and (8). The signal-to-noise level was investigated for the images. In our experiments the noise was in the range from −33 to −34 dB for incidence angles from 31° to 36°. This low noise level allowed a margin from 3 dB to 12 dB between the minimal signal in the slick and the noise after multilooking (see Table 1).

The Norwegian Clean Seas Association for Operating Companies conducts the annual oil-on-water exercises in the North Sea (centered at 59°59′N, 2°27′E). During the experiments carried out in 2011 and in 2012, crude oil, oil-in-water emulsions, and plant oil were released [*Skrunes et al*., 2012a, 2012b, 2014]. The plant oil was Radiagreen EBO (a monoalkyl ester of an oleic acid produced from vegetable oils; for details see *S2014*) used there to simulate natural monomolecular biogenic slicks.

The crude oil was the Balder crude oil. For summer conditions and a slick age of 9 h, which is approximately what we have in our SAR data, the water content is expected to be 21% (55%) under wind speeds of 2 m/s (5 m/s), respectively, (*S2014*). The Balder 2001 crude oil will produce stable emulsions with high viscosity, and a terminal slick thickness of 1 mm is predicted [*Moldestad and Schrader*, 2002].

The emulsion released in 2011 was composed of the Oseberg blend crude oil mixed with 5% of the intermediate fuel oil (IFO380) and water. It contained about 69% water. From boats close to the slick, the thickness of free-floating emulsion was estimated to be 0.1–1.5 mm (*S2014*). During the 2012 exercise, the emulsion was based on the same crude oil and had similar characteristics [*Skrunes et al*., 2015a].

The weather conditions were monitored from the ships participating in the exercise. The wind speed was about 1.5–3.3 m/s for the 2011 scene and 4 m/s for the 2012 scene.

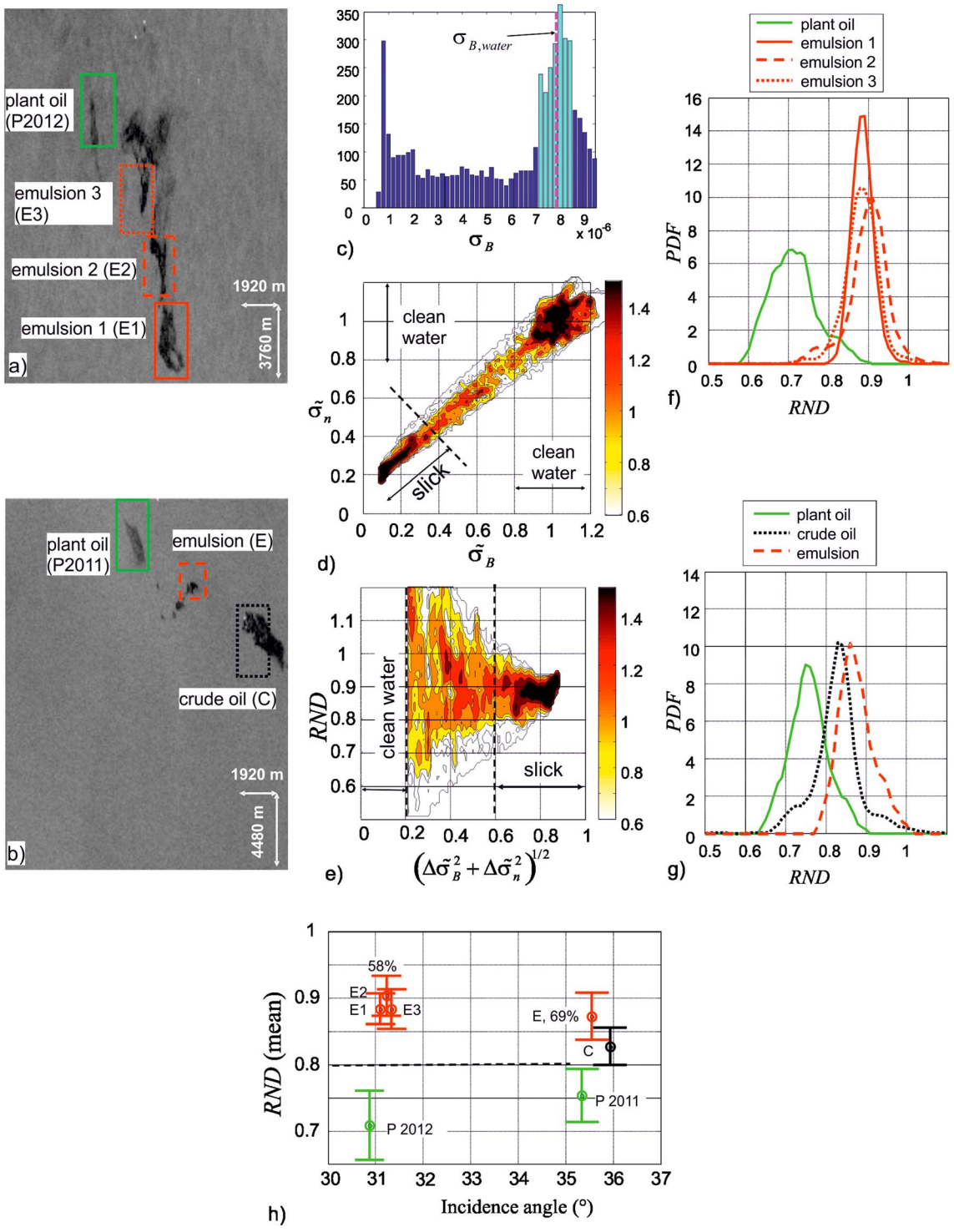

Figure 1. Subscenes of the RADARSAT-2 SAR images acquired: (a) on 15 June 2012, 6:20 UTC; (b) on 8 June 2011, 17:27 UTC. © MDA, KSAT. Azimuth and range scales shown at the right bottom corner of the scenes indicate the size of the rectangles containing slicks (excepting a small red rectangle with the emulsion in subscene Figure 1b). (c) Histogram of σ_B for "emulsion 2" from subscene Figure 1a. Light blue color marks the part of σ_B distribution taken by the centroid method for $\sigma_{B,\mathrm{water}}$ calculation. (d) Density plot of damping factors, $\tilde{\sigma}_B$, $\tilde{\sigma}_n$ for "emulsion 2" from subscene Figure 1a on a base 10 logarithmic scale. The color indicates the number of points. (e) Corresponding density plot for the (RND, $\left(\Delta\tilde{\sigma}_B^2+\Delta\tilde{\sigma}_n^2\right)^{1/2}$) domain. (f and g) RND probability density functions (PDF) for slicks in subscenes Figures 1a and 1b, respectively. (h) Summarizing plot of the mean RND ± one standard deviation (error bars) versus incidence angle.

Table 1. Processed Slicks and Inferred Corresponding Parameters

Slick Type, (Denotation)	Age, Water %[a]	Date, Image Pixel Spacing (Range × Azimuth), Wind Speed	Incidence Angle	Signal in Slick[b]: $\min(\sigma^H)$, *NESZ* (dB)	Signal in Slick[b]: $\min(\sigma^V)$, $\min(\sigma_n)$, $\sigma_{sp,typical}$[c], $(\sigma_{sp,max}$[d]) (dB)	Slick/Clean Water Maximal Contrast[b]: $\widetilde{\sigma}_B$, $\widetilde{\sigma}_n$ (dB)	RND (Mean ± SD)
Plant oil (P2011)	~13 h	8 June 2011, 17:27 UTC,	35.34°	−22.2, −23.4, −35.2	−26.9, −24.1, −94 (−70)	−8.4, −4.5	0.75 ± 0.04
Emulsion (E)	~29 h, 69%	4.7 × 4.8 m, 1.5–3.3 m/s	35.55°	−23.3, −25.1, −34.9	−26.7, −26.1, −96 (−71)	−7.5, −5.6	0.87 ± 0.04
Crude oil (C)	~9 h		35.93°	−27.5, −28.2, −33.9	−29.9, −28.6, −99 (−74)	−10.5, −7.5	0.83 ± 0.03
Plant oil(P2012)	~14 h	15 June 2012, 06:20 UTC,	30.87°	−22.7, −24.0, −35.2	−26.8, −25.3, −62 (−45)	−7.0, −4.0	0.71 ± 0.05
Emulsion 1 (E1)	~22 h, 58%	4.7 × 5.6 m, 4 m/s	31.10°	−25.0, −26.0, −35.5	−29.8, −26.9, −64 (−46)	−10.9, −7.4	0.88 ± 0.02
Emulsion 2 (E2)	~17 h, 58%		31.23°	−25.8, −26.9, −35.4	−30.4, −27.7, −65 (−47)	−11.6, −8.3	0.90 ± 0.03
Emulsion 3 (E3)	~14 h, 58%		31.33°	−24.8, −25.9, −35.4	−29.4, −26.7, −65 (−48)	−10.9, −8.0	0.88 ± 0.03

[a]Initial water contents at release time.
[b]For the chosen rectangle the minimum was calculated using smoothed image (near 500 m along slick and 120 m cross slick).
[c]$\sigma_{sp,typical}$ is for the slick upwind MSS by *Cox and Munk* [1954] and 6 m/s.
[d]$\sigma_{sp,max}$ is for the upwind MSS by *Hauser et al.* [2008] and 6 m/s.

4. Image Processing and Results

The subscenes of two processed images are shown in Figures 1a and 1b with range along the horizontal direction. For the processing we used a combination of initial spatial averaging and secondary window smoothing. Since the proposed method is based on the ratio (8) the final result is sensible to speckle noise variance. During the SAR image processing we tested several spatial averaging approaches and found well results using the following scheme. The intensity products of the VV and HH R-2 SAR images were multilooked by 8 points in each direction, resulting in the size of the processed image being reduced by a factor of 64. After that additional multilooking was done using a Hanning window of size 25 points in azimuth direction and a Hanning window of size 7 points in range direction. Asymmetric multilooking was chosen due to the slicks-elongated shape along azimuth. As a result, the final intensity values were obtained after approximately $3 \cdot 10^3$ noncoherent summations, which sufficiently improved the speckle noise variance of σ_B and σ_n. From empirical investigations, we found that such preprocessing provided the optimal balance between spatial smoothing (near 500 m along slick and 120 m cross slick) and a desired quality of the final parameter estimates (meaning its standard deviation).

In each scene, we chose the regions of interest (indicated by rectangles in Figures 1a and 1b) in such a way that they contain both a slick and clean water. The histogram of σ_B points for the 2012 E1 is shown in Figure 1c. $\sigma_{B,\text{water}}$ value was calculated on the basis of these points using the centroid method [*Barrick*, 1980]. According to the centroid method practice, the cutoff of one half of the maximum of the histogram height was applied to separate the clean water points lying near the most probable value of σ_B for the clean water. The same procedure was applied for $\sigma_{n,\text{water}}$. Then, for each point within the region, we calculated the damping factors, $\widetilde{\sigma}_B$ and $\widetilde{\sigma}_n$, from (6), for resonant and nonresonant signals and plotted them into the coordinate plane $[\widetilde{\sigma}_B,\ \widetilde{\sigma}_n]$. Subsequently, we calculated the point density on a unit area (applying a size of 0.02×0.02 in the $[\widetilde{\sigma}_B,\ \widetilde{\sigma}_n]$ domain). We stress that all these steps, after choosing the regions of interest, were performed automatically.

Figure 1d shows an example of $[\widetilde{\sigma}_B,\ \widetilde{\sigma}_n]$ distribution for the region containing "emulsion 1" from Figure 1a. According to the normalization in (6), most of the points corresponding to the clean water are located near the unity in each direction, i.e., resonant and nonresonant components. Damping factors below a threshold of 0.6 (i.e., $\left[\Delta\widetilde{\sigma}_B^2 + \Delta\widetilde{\sigma}_n^2\right]^{1/2} > 0.6$) are considered to be related to the slick (as shown in Figure 1d). We do not have detailed information about thickness variations, but damping factors attributed to the slicks vary significantly

by a factor of 5 for the Bragg component (from 0.5 to 0.1 for $\widetilde{\sigma}_B$) and similar for the nonresonant component (from 0.5 to 0.2 for $\widetilde{\sigma}_n$). We can attribute these variations to the thickness variations mainly. Partially, some $\widetilde{\sigma}_B$ and $\widetilde{\sigma}_n$ variations at the slick edges might be caused by the spatial smoothing of the image. At the same time, the maximal $\widetilde{\sigma}_B$ and $\widetilde{\sigma}_n$ contrasts within the oil slick were reduced because of the same image smoothing.

The most important point for our analysis is that the density distribution of $\widetilde{\sigma}_B$, $\widetilde{\sigma}_n$ within the slick has a form of a narrow and approximate straight line with minor deviations. This fact allows to justify our assumption that the parameter RND defined in (8) should not vary much in the range of typical thicknesses for one slick type (see Figure 1e) for the corresponding density distribution of RND, $\left(\Delta\widetilde{\sigma}_B^2 + \Delta\widetilde{\sigma}_n^2\right)^{1/2}$.

An additional benefit of using the RND parameter, possessing the favorable property of remaining nearly constant within the slick, is that it is possible to use most of the points within the slick to compose the 1-D density distribution for RND and derive robust estimates for its first statistical moments, i.e., the mean and standard deviation. We used all the RND points in the region $\left(\Delta\widetilde{\sigma}_B^2 + \Delta\widetilde{\sigma}_n^2\right)^{1/2} > 0.6$ of sufficiently strong signal damping (see indication slick in Figure 1e). After summing all these points the 1-D probability distribution function of RND was obtained (see Figure 1f). The same processing was applied for all target regions; the resulting probability distributions are shown in Figures 1f and 1g.

The probability distributions in Figures 1f and 1g have a shape similar to the Gaussian distribution with one distinct maximum. For the scene on 15 June 2012, the probability distribution of RND for the plant oil lies at smaller values of RND than that of the three emulsions (Figure 1f). The plant oil RND distribution is well separated from the emulsion RND distributions. The two emulsions are placed almost at the same position and are undistinguishable from one another. An analogous picture is seen for the scene from 8 June 2011, as shown in Figure 1g. The RND for the plant oil is also separated (in terms of the mean standard deviation) from the emulsion and crude oil RND; the latter two are undistinguishable from one another (in terms of the mean standard deviation).

The summarized results for the analyzed seven slick patches are presented in Table 1 and Figure 1h. The local incidence angle, which varies from 31° to 36°, is shown along the *x* axis. It is seen that the mean RND values for the emulsions and crude oil are separated (in terms of the mean standard deviation) from the mean RND for the plant oil slicks. A RND value of 0.8 (indicated by the dashed line) could serve as a threshold line between the plant oil slicks and the mineral oil slicks. The crude oil is not clearly discernible from the emulsion class (as have also been found in other papers (*S*2014, *S*2015b) using different polarimetric parameters). As the crude oil has been on the surface for about 9 h, it has been subjected to various weathering mechanisms, e.g., emulsification, and may also be an emulsion at the time of the SAR acquisition. This may be why this release is not discernible from the released emulsions.

The technique demonstrated desired small variations of the target parameter RND within the tested range of incidence angles of 31°–36°. While the corresponding Bragg wave number had changed 14%, the parameter RND for emulsions had changed 3% (for comparison, for the same images and oil slicks the Touzi scattering phase had changed 20%, the entropy 13% [*Staples*, 2015]).

An important result concerns a great role of the nonresonant backscattering σ_n in the copolarized signals σ^V and σ^H. In our examples of incidence angles of 31°–36° and winds 1.5–4 m/s, in the slicks σ_n contributes more than 50% to σ^V (see Table 1) and, correspondingly, more than 70% to σ^H (taking into account $P_{0B} < 0.4$ for angles >30°). In the clean water σ_n contributes more than 40% to σ^V and more than 60% to σ^H.

5. Analysis of Minimal Incidence Angle

A simple estimate for the possible minimal incidence angle, at which the proposed technique is valid, can be done using the mean square slope (MSS) functional forms inferred (i) in the work by *Cox and Munk* [1954] from optical glitter measurements and (ii) in *Hauser et al*. [2008] from C band airborne radar data [*Mouche et al*., 2005]. Since the radar filters out the properties of the waves shorter than a certain limit, k_d [*Thompson et al*., 2005] (say, $k_d = 51$ rad/m for clean water and $k_d = 16.5$ rad/m for the Cox and Munk slick data [*Hauser et al*., 2008]) the slick MSS by *Cox and Munk* [1954] was considered as a reasonable estimate for typical radar-filtered MSS in the slick surface, and the clean C band MSS by *Thompson et al*. [2005] was considered as a conservative estimate for maximal possible radar-filtered MSS in the slick surface. In addition, we used

greater of two MSSs, the upwind/downwind MSSs. For the wind speeds less than 6 m/s these typical and maximal radar-filtered MSSs in the slick result in 0.0097 and 0.0125, correspondingly [see *Hauser et al*., 2008, Figure 6a]. For angles 31°–36° it means that the specular part, σ_{sp}, is several orders lower (from −10 to −40 dB; see Table 1) than the nonresonant part, σ_n.

As to the smaller angles, analogous estimates for typical and maximal specular reflections in the slick at the incidence angle 27° result in $\sigma_{sp,typical} < -41$ dB and $\sigma_{sp,max} < -29$ dB. The minimal σ_n values from Table 1 (−28.7 dB at 35.93° and −26.9 dB at 31.1°) observed for light winds about 1.5–3.3 m/s can be recalculated following formula (4) as they would be acquired at the incidence angle 27°, which results in −24.4 dB and −25.2 dB, correspondingly. Therefore, this conservative estimate says that for incidence angles greater than 27° and winds less than 6 m/s the nonresonant part of the signal σ_n at C band has to remain greater than 4 dB in the slick than the specular reflections σ_{sp} dB. We used value less than 6 m/s as very typical for slick observation in SAR images, but following this approach analogous estimates can be done for other wind speeds and incidence angles. Merely, at high angles (>40°–45°), the minimal signal in the slick could approach the noise floor, which could distort processing results.

6. Conclusion

A simple copolarization technique has been proposed for processing of multipolarization SAR images aiming at discriminating surface slicks, such as mineral oils (e.g., emulsion and crude oil) versus natural slicks. The technique is based on the model of the electromagnetic scattering on the sea surface proposed by *Kudryavtsev et al*. [2003a] and has a physical comprehensible basis. In this paper we confined our consideration to surface slicks with thicknesses less than the radio wave skin depth that excluded the dependence of the technique on the dielectric constant of oil. To demonstrate advantages of the model application, a simplistic case was considered when the Kirchhoff reflections from the slopes of long wind waves can be neglected.

For distinguishing of different types of slicks on SAR images, we introduced a parameter called "the ratio of the resonant and nonresonant components relative damping" or RND. This *quantitative* parameter appeared as a logical derivation of *qualitative* considerations presented in *K*2013 and *S2015b* about different ratios of damping of breaking and Bragg waves in different slicks. It is crucial for operational purposes that the parameter RND can be automatically calculated during the processing of SAR subscenes containing slicks, and by derivation it should not vary significantly with the incidence angle.

This technique was tested on RADARSAT-2 SAR images acquired over oil-on-water exercises in the North Sea, containing oil slicks of various origins: crude oil, oil emulsion, and plant oil. By processing seven dark spots from various slick types, it has been demonstrated that the proposed method can allow confident discrimination of plant oil (which was used to simulate monomolecular biogenic films) from crude oil and mineral oil emulsions. The different mineral oils (crude oil and its emulsions) could not be distinguished from each other, as has also been found in *S*2014 and *S*2015b that used other polarimetric methods (e.g., geometric intensity and real part of the copolarization cross product). The technique demonstrated desired robustness within the tested range of incidence angles of 31°–36°: while the corresponding Bragg wave number changed 14%, the parameter RND for emulsions changed 3%. The technique does not require complex data but intensity only. Therefore, both the single look complex (SLC) and ground-projected intensity can be used.

Conservative estimates using MSS by *Cox and Munk* [1954] and *Hauser et al*. [2008] have shown that assumption about the negligible effect to our technique of the Kirchhoff reflections from the slopes of long wind waves is valid for SAR images acquired at incidence angles exceeding 27° and wind speeds less than 6 m/s. For other wind conditions the corresponding limitations can be easily obtained using our proposed checkup procedure.

It was shown an important role of the nonresonant backscattering due to wave breakings and microbreakings that could contribute 40%–70% to copolarized NRCS. In the slicks the nonresonant backscattering due to wave breakings was damped 4–8 dB, while the resonant Bragg backscattering was damped 7–11 dB.

A significant requirement for successful application of the technique was processing of low-noise SAR data with margin greater than 3 dB between the noise and minimal signal in the slick. Note that even though this technique uses only the copolarization channels, the noise may still be a problem for current space-borne SAR systems at higher incidence angles and in low wind speed conditions.

The technique has a good potential for improvement and development due to its direct quantitative relationship to parameters of the scattering model, for example, in the direction of removing limitations for the technique on the incidence angles, getting a more nuanced classification of sea surface slicks, for generalizing the method to other data, e.g., TerraSAR-X, for a multifrequency slick analysis, and for a reduction of the noise.

Acknowledgments
Exclusive owner of the RADARSAT-2 data and products is MacDonald, Dettwiler and Associates Ltd. (MDA). The RADARSAT-2 data over the North Sea in 2011 were provided by the Norwegian Space Centre/Kongsberg Satellite Services under the Norwegian-Canadian Radarsat agreement 2011. The RADARSAT-2 data over the North Sea in 2012 were funded by Total E&P Norge AS and Total S.A. RADARSAT-2 Data and Products © MacDonald, Dettwiler and Associated Ltd., 2011 and 2012—All rights reserved. This work was supported by the Russian Foundation for Basic Research, project 14-05-93084 and by the Norwegian Research Council through the BIA project 235444 and the NORRUSS project 233896. We thank V.N. Kudryavtsev and V.I. Shrira for useful comments.

References

Banner, M. L., and E. H. Fooks (1985), On the microwave reflectivity of small-scale breaking water waves, *Proc. R. Soc. London Ser. A.*, *399*(1816), 93–109.

Barrick, D. E. (1980), Accuracy of parameter extraction from sample-averaged sea-echo Doppler spectra, *IEEE Trans. Antennas Propag.*, *28*(1), 1–11.

Caulliez, G. (2013), Dissipation regimes for short wind waves, *J. Geophys. Res. Oceans*, *118*, 672–684, doi:10.1029/2012JC008402.

Caulliez, G., and C. A. Guérin (2012), Higher-order statistical analysis of short wind wave fields, *J. Geophys. Res.*, *117*, C06002, doi:10.1029/2011JC007854.

Churyumov, A. N., Y. A. Kravtsov, O. Y. Lavrova, K. T. Litovchenko, M. I. Mityagina, and K. D. Sabinin (2002), Signatures of resonant and non-resonant scattering mechanisms on radar images of internal waves, *Int. J. Remote Sens.*, *23*(20), 4341–4355.

Cox, C., and W. Munk (1954), Measurement of the roughness of the sea surface from photographs of the Sun's glitter, *J. Opt. Soc. Am.*, *44*(11), 838–850.

Elfouhaily, T., B. Chapron, K. Katsaros, and D. Vandemark (1997), A unified directional spectrum for long and short wind-driven waves, *J. Geophys. Res.*, *102*, 15,781–15,796, doi:10.1029/97JC00467.

Ericson, E. A., D. R. Lyzenga, and D. T. Walker (1999), Radar backscattering from stationary breaking waves, *J. Geophys. Res.*, *104*, 29,679–29,695, doi:10.1029/1999JC900223.

Franceschetti, G., A. Iodice, D. Riccio, G. Ruello, and R. Siviero (2002), SAR raw signal simulation of oil slicks in ocean environments, *IEEE Trans. Geosci. Remote Sens.*, *40*(9), 1935–1949.

Gade, M., W. Alpers, H. Hühnerfuss, and P. A. Lange (1998a), Wind wave tank measurements of wave damping and radar cross sections in the presence of monomolecular surface films, *J. Geophys. Res.*, *103*(C2), 3167–3178, doi:10.1029/97JC01578.

Gade, M., W. Alpers, H. Hühnerfuss, H. Masuko, and T. Kobayashi (1998b), Imaging of biogenic and anthropogenic ocean surface films by the multifrequency/multipolarization SIR-C/X-SAR, *J. Geophys. Res.*, *103*, 18,851–18,866, doi:10.1029/97JC01915.

Guérin, C. A., G. Soriano, and B. Chapron (2010), The weighted curvature approximation in scattering from sea surfaces, *Waves Random Complex Media*, *20*(3), 364–384.

Hauser, D., G. Caudal, S. Guimbard, and A. A. Mouche (2008), A study of the slope probability density function of the ocean waves from radar observations, *J. Geophys. Res.*, *113*, C02006, doi:10.1029/2007JC004264.

Kudryavtsev, V., D. Hauser, G. Caudal, and B. Chapron (2003a), A semiempirical model of the normalized radar cross-section of the sea surface: 1. Background model, *J. Geophys. Res.*, *108*(C3), 8054, doi:10.1029/2001JC001003.

Kudryavtsev, V., D. Hauser, G. Caudal, and B. Chapron (2003b), A semiempirical model of the normalized radar cross-section of the sea surface: 2. Radar modulation transfer function, *J. Geophys. Res.*, *108*(C3), 8055, doi:10.1029/2001JC001004.

Kudryavtsev, V. N., B. Chapron, A. G. Myasoedov, F. Collard, and J. A. Johannessen (2013), On dual co-polarized SAR measurements of the ocean surface, *IEEE Geosci. Remote Sens. Lett.*, *10*(4), 761–765.

Kwoh, D. S., and B. M. Lake (1984), A deterministic, coherent, and dual-polarized laboratory study of microwave backscattering from water waves: 1. Short gravity waves without wind, *IEEE J. Oceanic Eng.*, *9*, 291–308.

MDA (MacDonald, Dettwiler and Associates Ltd.), Geospatial Service (2014), RADARSAT-2 product description, RN-SP-52-1238, Issue 1/11: 5 May.

Migliaccio, M., F. Nunziata, and A. Gambardella (2009), On the co-polarized phase difference for oil spill observation, *Int. J. Remote Sens.*, *30*(6), 1587–1602.

Minchew, B., C. E. Jones, and B. Holt (2012), Polarimetric analysis of backscatter from the Deepwater Horizon oil spill using L-band synthetic aperture radar, *IEEE Trans. Geosci. Remote Sens.*, *50*(10), 3812–3830.

Moldestad, M. Ø., and T. Schrader (2002), ESSO BJR9: Ringhorne, Forseti og Balder; Egenskaper og Forvitring på Sjøen Relatert til Beredskap SINTEF, Trondheim, Norway, Tech. Rep. STF66 A01137.

Mouche, A. A., D. Hauser, J.-F. Daloze, and C. Guérin (2005), Dual-polarisation measurements at C-Band over the ocean: Results from airborne radar observations and comparison with ENVISAT ASAR data, *IEEE Trans. Geosci. Remote Sens.*, *43*(4), 753–769.

North, E. W., E. E. Adams, Z. Schlag, C. R. Sherwood, R. He, K. H. Hyun, and S. A. Socolofsky (2011), Simulating oil droplet dispersal from the Deepwater Horizon spill with a Lagrangian approach, in *Monitoring and Modeling of the Deepwater Horizon Oil Spill: A Record-Breaking Enterprise*, edited by Y. Liu et al., pp. 217–226, AGU, Washington, D. C.

Phillips, O. M. (1988), Radar returns from the sea surface Bragg scattering and breaking waves, *J. Phys. Oceanogr.*, *18*, 1063–1074.

Skrunes, S., C. Brekke, and T. Eltoft (2012a), Oil spill characterization with multi-polarization C- and X-band SAR, in *Proc. of the Geoscience and Remote Sensing Symposium (IGARSS-2012), IEEE International*, pp. 5117–5120, IEEE, Munich.

Skrunes, S., C. Brekke, and T. Eltoft (2012b), An experimental study on oil spill characterization by multipolarization SAR, in *Proc. of the 9th European Conference on Synthetic Aperture Radar (EUSAR-2012)*, pp. 139–142, VDE, Nuremberg, Germany.

Skrunes, S., C. Brekke, and T. Eltoft (2014), Characterization of marine surface slicks by Radarsat-2 multipolarization features, *IEEE Trans. Geosci. Remote Sens.*, *52*(9), 5302–5319.

Skrunes, S., C. Brekke, and A. P. Doulgeris (2015a), Characterization of low-backscatter ocean features in dual-copolarization SAR using log-cumulants, *IEEE Geosci. Remote Sens. Lett.*, *12*(4), 836–840.

Skrunes, S., C. Brekke, T. Eltoft, and V. Kudryavtsev (2015b), Comparing near coincident C- and X-band SAR acquisitions of marine oil spills, *IEEE Trans. Geosci. Remote Sens.*, *53*(4), 1958–1975.

Staples, G. (2015), Oil slick discrimination using RADARSAT-2 quad polarized data Paper presented at Geoscience and Remote Sensing Symposium (IGARSS), 2015 IEEE International, Milan, Italy.

Thompson, D. R., T. M. Elfouhaily, and J. L. Garrison (2005), An improved geometrical optics model for bistatic GPS scattering from the ocean surface, *IEEE Trans. Geosci. Remote Sens.*, *43*(12), 2810–2821, doi:10.1109/TGRS.2005.857895.

Ulaby, F. T., R. K. Moore, and A. K. Fung (1986), *Microwave Remote Sensing: Active and Passive*, Artech House, Dedham, Mass.

Valenzuela, G. R. (1978), Theories for the interaction of electromagnetic and ocean waves—A review, *Boundary Layer Meteorol.*, *13*, 61–85.
Velotto, D., M. Migliaccio, F. Nunziata, and S. Lehner (2011), Dual-polarized TerraSAR-X data for oil-spill observation, *IEEE Trans. Geosci. Remote Sens.*, *49*(12), 4751–4762.
Yurovskaya, M. V., V. A. Dulov, B. Chapron, and V. N. Kudryavtsev (2013), Directional short wind wave spectra derived from the sea surface photography, *J. Geophys. Res. Oceans*, *118*, 4380–4394, doi:10.1002/jgrc.20296.
Zhang, B., W. Perrie, X. Li, and W. G. Pichel (2011), Mapping sea surface oil slicks using RADARSAT-2 quad-polarization SAR image, *Geophys. Res. Lett.*, *38*, L10602, doi:10.1029/2011GL047013.